THE ASTROPHYSICAL JOURNAL, 330:385–398, 1988 July 1

L43: AN EXAMPLE OF INTERACTION BETWEEN MOLECULAR OUTFLOWS AND DENSE CORES

ROBERT D. MATHIEU,[1] PRISCILLA J. BENSON,[2,3] GARY A. FULLER,[1,4] PHILIP C. MYERS,[1] AND RUDOLPH E. SCHILD[1]

Received 1987 August 3; accepted 1987 December 17

ABSTRACT

Images of the dark cloud L43 and the associated young star RNO 91 in the red continuum and in millimeter wavelength lines reveal a dense core being disrupted by the action of a molecular outflow. CCD images reveal a bay around RNO 91 delineated by higher surface luminosity within and reflection nebulosity along its borders. The blue lobe of the associated ^{12}CO outflow is coincident with this bay in projection. NH_3 emission closely follows the high extinction adjacent to the bay; within the bay NH_3 is detected only in the vicinity of RNO 91. RNO 91 is displaced by 0.07 pc from the NH_3 peak. The distribution of CS emission also follows the extinction but does not reflect the structure of the bay and outflow. The CS emission is approximately 50% more extended than the NH_3 emission, despite the similarity in critical density of the CS and NH_3 lines.

Both the NH_3 and CS line widths increase within the boundaries of the outflow. The two regions of greatest line width are 0.15 pc distant from RNO 91, projected on the red and blue outflow lobes. There is a 2 km s^{-1} pc^{-1} velocity gradient in both the NH_3 and CS velocity fields within 0.1 pc of RNO 91. If the gradient is due to rotation, the projected angular momentum vector is roughly orthogonal to the projected axis of the outflow.

The coincidence of the bay and the molecular outflow, the morphology of the NH_3 emission, and the increase in line widths within the bay form a coherent picture in which the outflow, originating at RNO 91, has blown through the dense core into the lower density environs, in the process revealing the star and the outflow cavity. These data show that outflows can be sufficiently coupled to the dense cores in which they form so as to substantially alter their structure. However, in L43 the modification of the core structure and the increase in internal motions presently are found only within a limited volume of the core; the dense gas surrounding the bay is typical of quiescent cores without embedded stars.

Finally, small-scale CCD images of RNO 91 reveal an elongated feature 1000 AU in length, with an alignment similar to the axis of the outflow in the direction of the blue lobe. Two other smaller elongated features, as well a string of knots, are also found adjacent to RNO 91. These features are evident in *I* band images and are not enhanced at Hα, suggesting that the luminosity is primarily reflected light.

Subject headings: interstellar: molecules — nebulae: individual

I. INTRODUCTION

There is now substantial evidence that low-mass stars form in dense molecular cores in dark clouds (Myers 1985). Ultimately these stars disassociate themselves from their parent gas. Whether this disassociation occurs through complete consumption of the core, disruption of the core by stellar winds or other outflows, motion of the star relative to the gas, or some other mechanism is not yet clear. We discuss here observations of a core in the dark cloud L43 whose structure is at the moment being substantially altered by the action of a molecular outflow associated with a young star.

L43 is an elongated dark cloud with dimensions of roughly 1.7 pc by 0.3 pc (Herbst and Warner 1981). It is projected upon and presumably associated with the Sco OB2 complex at a distance of 160 pc. The cloud was mapped in CO by Elmegreen and Elmegreen (1979) who found the molecular cloud to extend roughly twice as far as the extinction in all directions. They noted the presence of an elongated core near the center of the cloud, with a total mass of greater than 14 $M_\odot$ deduced from ^{12}CO and ^{13}CO measurements. Observations in H_2CO by Loren (1981) indicated a density in this core of 1.5×10^5 cm^{-3}, from which he conjectured that the core was a likely site of star formation. Myers, Linke, and Benson (1983) identified two opaque spots in the core. Associated NH_3 emission was later detected by Myers and Benson (1983), indicating the presence of a dense molecular core with a mass of 0.7 $M_\odot$. Finally, Levreault (1988) and Myers *et al.* (1988) have detected a weak CO outflow associated with this core.

Elmegreen and Elmegreen (1979) noted the presence of two stars associated with L43, as indicated by reflection nebulosity. These were cataloged in Cohen's (1980) list of red nebulous objects as RNO 90 and 91. Herbst and Warner (1981) obtained optical and infrared photometry of both sources and a spectrogram of the brighter, RNO 90, which identified it as a T Tauri star. Levreault (1988) classified RNO 91 as a T Tauri star of spectral type M0.5 and noted that its location in the color-magnitude diagram near the birthline of Stahler (1985) indicates a very young age, of order 10^5 yr. *IRAS* observations revealed a point source, 16316−1540, within the dense core and associated with RNO 91 (Beichman *et al.* 1986). The *IRAS*

[1] Harvard-Smithsonian Center for Astrophysics.
[2] Department of Astronomy, Wellesley College.
[3] Guest Observer, MPIFR.
[4] Astronomy Department and Radio Astronomy Laboratory, University of California, Berkeley.

fluxes from 12 to 100 μm indicate a steeper spectral slope than typical for the visible T Tauri stars included in Beichman *et al.* Further study of this source in the near-infrared and optical by Myers *et al.* (1987) confirmed the association with RNO 91 and showed the source to be of only moderately steep spectral slope in the near-infrared, more typical of other visible T Tauri stars included in their study. Myers *et al.* derive a bolometric luminosity of 4.3 $L_{\odot}$.

Thus the vicinity of RNO 91 in L43 includes an extensive inventory of those phenomena associated with low-mass star formation: a visible young stellar object, a dense molecular core in a more extended dark cloud, a molecular outflow, and diffuse nebulosity. It joins a rapidly increasing number of regions in which careful optical studies have revealed optical arcs, fans, and other nebulous features closely associated with observed molecular outflows (see, e.g., Levreault 1984; Snell *et al.* 1985; Campbell, Persson, and MacGregor 1986; Strom *et al.* 1986). Because of a favorable orientation, the simple structure of the surrounding molecular cloud, and its relative proximity to Earth, the morphology of the L43 region is particularly accessible to optical study. In particular, the volume containing the blueshifted lobe of the molecular outflow is fully exposed, allowing detailed study of the interaction of the outflow with the cloud. As such, L43 presents an unusually good example of the mechanism by which molecular outflows modify and disturb the environment of a newly formed star.

In this paper we first describe the observations (§ II) and then discuss in detail the morphology of the region (§ III). The most striking feature on CCD images is a bay in the dark cloud; RNO 91 lies near the closed end of this bay. The blueshifted lobe of the molecular outflow is coincident with the bay in projection, while the complex of RNO 91, the bay, and the outflow lie somewhat removed from the peak of the dense molecular core. This morphological evidence for interaction between the outflow and the cloud is reinforced by analysis of the gas kinematics of the region (§ IV). Both NH_3 and CS emission show a substantial increase in line width within the confines of the bay and outflow. In addition, the velocity field has a steep gradient centered on RNO 91. In § V we discuss these results in light of recent suggestions that molecular outflows disrupt cores. Substantial modification of the L43 core structure has already occurred. However, only a limited volume of the dense molecular core surrounding RNO 91 has been disturbed; that portion of the molecular core external to the outflow volume is typical of quiescent cores without associated young stellar objects.

II. OBSERVATIONS

Optical data were obtained at the Fred L. Whipple Observatory 61 cm telescope with the RCA CCD camera (Geary and Kent 1981; bandpasses defined in Schild and Kent 1981) at the Cassegrain focus. Two 20 minute integrations in the *I* bandpass were obtained on 1986 May 29 at 1.46 arcsec mm^{-1}. These large-scale images were offset from each other in the north/south direction. The frames were then combined to create a 512 × 512 pixel image covering 12.4 arcmin square 0.6 pc square at L43. Thirty-minute integrations were also obtained in the *F* and *I* bandpasses, as well as in a narrow-band (FWHM = 100 Å) Hα filter, on 1987 April 13 at a scale of 0.73 arcsec mm^{-1}, giving sky coverage of 3.'9 by 6.'2 or 0.2 by 0.3 pc at the distance of L43. The seeing both nights was 1″. All frames were flat-fielded with dome flats, corrected for fringing with night sky fields and edited of cosmic rays and chip flaws. The *I* bandpass does not admit emission lines found to be strong in shocked environments of star-forming regions (e.g., in Herbig-Haro objects), thus the *I* images map scattered light. The *F* bandpass includes Hα and several strong forbidden emission lines as well as scattered light. The Hα filter admits primarily Hα and the [N II] lines.

A map of the molecular core in the NH_3 $(J, K) = (1, 1)$ line at 1.3 cm wavelength was made at the 37 m telescope of Haystack Observatory in the summer of 1985. Beam spacing was 1′, somewhat less than the Haystack FWHM beam diameter of 1.'4, with offsets taken from the *IRAS* source position ($16^h31^m37^s.9$, −15°40′50″ [1950]). The spectrometer was a 1024 channel autocorrelator with a bandwidth of 5.55 MHz and velocity resolution of 0.8 km s^{-1}. All spectra were corrected for atmospheric attenuation and variations in gain with elevation. The typical rms variation in one channel was 0.1 K. Reductions followed the procedures detailed in Benson and Myers (1980).

Higher spatial resolution observations in both the NH_3 $(J, K) = (1, 1)$ and (2, 2) lines were also made with the 100 m Effelsberg telescope of the Max Planck Institut für Radioastronomie in the summer of 1984. The Effelsberg observations surveyed only the central region of the NH_3 core. Eight positions were observed along a constant declination track passing from 0.'5 west to 3′ east of the *IRAS* position. Observations were also made at the six westmost positions along parallel tracks 0.'5 north and south of the central track. Beam spacing was 0.'5, comparable to the beam diameter of 0.'67. The $(J, K) = (1, 1)$ and $(J, K) = (2, 2)$ lines were observed simultaneously with the 1024 channel autocorrelator split into two 512 channel sections. A bandwidth of 1.56 MHz in each section gave a velocity resolution of 0.5 km s^{-1}. This showed the central 14 of the 18 hyperfine components of the (1, 1) line. The spectra were scaled to brightness temperatures T_A^* with corrections for atmospheric effects and variation in gain of the telescope with elevation based on observations of NGC 7027. The typical rms variation in one channel was 0.5 K.

The CS $J = 2$–1 line observations at 3.0 mm were made at the NRAO[5] 12 m telescope at Kitt Peak in 1986 October. The beam diameter was 64″ and the antenna temperature calibrated using the usual chopper wheel method (Kutner and Ulich 1981). The dual polarization receiver was used to feed two 100 kHz filter banks giving a velocity resolution of 0.31 km s^{-1}. The spectra from these two banks were then averaged, weighted by their system temperatures. First, and occasionally second, order baselines were removed from the spectra before analysis. The typical rms variation in one channel was $T_R^* =$ 0.1 K. A nearly complete map was made over a 6′ by 10′ region with 1′ spacing, centered on a position 1′ east of RNO 91.

III. THE MORPHOLOGY OF THE L43B REGION

On the POSS red plate the L43 dark cloud appears to have a filamentary structure, approximately 1.7 by 0.3 parsecs in size. At the center of the filament is a highly obscured region[6] near which is projected the T Tauri star RNO 91. Another T Tauri star, RNO 90, lies about 5′ to the west of RNO 91. Both stars have associated nebulosity. RNO 91 lies within a parabolic-shaped region of lower extinction and higher surface brightness than elsewhere in the filament, which we hereafter

[5] The National Radio Astronomy Observatory is operated by Associated Universities, Inc., under contract with the National Science Foundation.

refer to as the "bay." The bay opens to the south while RNO 91 lies near the closed end to the north, which we hereafter call the "rear" of the bay. The morphology and kinematics within this bay are the focus of the following discussion. In this section we first point out the essential morphological details and then provide a model for the structure of the region.

The bay is only marginally discernible on the POSS but is clearly evident on the large-scale CCD *I* band image of the region, shown in Figure 1 (Plate 13). Two regions of very high extinction are evident to the east and west of RNO 91, connected by a thin strip of obscuration passing to the north of RNO 91. These serve to outline the bay. The surface brightness within the bay is higher than in the regions of high extinction. While a few visible stars are projected within the bay, the stellar surface density is an order of magnitude less than in the star field to the northwest. The small number of stars and the enhanced surface brightness within the bay make an accurate determination of the extinction difficult, but qualitatively the extinction along the line of sight to the bay appears to be less than in the immediately adjacent regions of high extinction but greater than regions outside the filamentary cloud.

The surface brightness within the bay is approximately uniform, excepting the enhanced surface brightness of the nebulosity along the eastern wall and at the northern end of the bay. Interestingly, the surface brightness within the bay extends from the mouth of the bay southward beyond the boundaries of the immediately adjacent filament. The brightest nebulosity lies at the northern end of the bay. The more extensive nebulosity to the west is curved and comprises one arc of the wall of the bay. A more compact, oval-shaped region of nebulosity of comparable brightness lies in the interior of the northern end of the bay. RNO 91 is embedded in the western end of this oval. As there is no enhancement of any of the nebulosity relative to RNO 91 among the *F*, *I*, and Hα frames, the nebulae are all presumably illuminated by reflected light from RNO 91.

The small-scale higher resolution CCD frames reveal extensive structure in the nebulosity immediately surrounding RNO 91; a portion of the *I* frame is shown in Figure 2 (Plate 14). Most notable is the elongated feature extending radially to the south of RNO 91. We have confirmed that the feature is not an artifact by (1) comparing the images of RNO 90 and 91 on the large-scale CCD frame and (2) noting an extension of the RNO 91 image to the south on the POSS red print. The elongated feature is separated from the star by a dark strip roughly 2″ (300 AU) wide. The length of the feature is 7″ (1100 AU); it is unresolved in width. The orientation of the feature is roughly aligned with the bay and the blue lobe of the ^{12}CO outflow (discussed below).

Morphologically this feature bears a resemblance to the shock-excited jets found around other very young stars (see, e.g., Mundt 1985). However, the surface brightness of the feature in the *I* bandpass suggests that reflected light is a substantial component of the luminosity. Indeed, there are no significant differences in the relative surface density distributions in the *F*, *I*, and Hα images. Thus there is no evidence for shock-excited emission and we conclude that the luminosity is dominated by scattered light from RNO 91.

Detailed examination of intensity profiles through the center of the stellar image reveal additional extended emission in all directions. Of particular note are two additional elongated features to the northwest and southwest of the star, evident in Figure 2. In each case the features are not as well aligned with the center of the stellar image nor as long as the feature to the south. Finally, we draw attention to a series of approximately aligned knots of luminosity to the west of RNO 91, oriented along the axis of the bay. While reminiscent of Herbig-Haro objects, these knots also show no relative enhancement in the Hα frame and their orientation with respect to the star is not typical of H-H objects so that again they are likely to be reflected light. All of these features suggest the presence of a great deal of structure and clumpiness in the material surrounding RNO 91.

The addition of the molecular-line data provides greater richness to the panorama. In Figure 3 we again present the large-scale *I*-band CCD frame, upon which we have superposed contour maps derived from the ^{12}CO, NH_3, and CS data. The ^{12}CO $J = 1$–0 integrated line-wing intensity has been taken from Myers *et al.* (1988). The NH_3 $(J, K) = (1, 1)$ contours, derived from the Haystack observations, indicate the peak line intensity T_A^* of the main hyperfine component (derived as in Myers and Benson 1983). The CS (2–1) contours indicate peak line intensity T_R^*, determined from Gaussian fits to the line profiles.

The most notable coincidence of molecular line data and the optical image is that of the CO blue-wing emission with the bay, shown in Figure 3*a*. The strongest blue-wing emission is centrally located at the rear of the bay, not far removed from RNO 91. Along the boundaries of the bay the CO emission decreases abruptly, so that little high-velocity emission is found projected upon the obscuration immediately outside the walls of the bay. The only extension of the CO emission is out the mouth of the bay, where low-intensity emission extends beyond the southern limit of the high extinction. This weak CO coincides with the extended optical surface brightness noted above. There is little evidence for any morphology in the optical data which coincides with the structure of the red-wing emission, although the western boundary of the eastern extinction coincides with the boundary of the red-wing emission. Since much of the red-wing CO emission is projected upon a region of high extinction, the lack of corresponding optical structure may simply be due to such features being hidden behind the extinction. It is worth noting, though, that the red-wing emission projects to the north beyond the limits of the high extinction, with no evident coincident enhancement in surface brightness.

The map of NH_3 antenna temperature (Fig. 3*b*) presents a very different morphology from that of the ^{12}CO wing map. Around both RNO 91 and RNO 90 the Haystack observations were extended until the peak line intensity T_A^* dropped to below $\sim$0.15 K. Thus most of the NH_3 emission lies within the contours shown in Figure 3*b*. The peak of the NH_3 emission is projected upon the eastern wall of the bay, 0.07 pc distant from RNO 91. To the east and west of the bay the NH_3 emission is, in projection, coincident with the regions of high extinction. The NH_3 emission decreases at the bay boundary, and within the bay little emission is detected away from RNO 91. Indeed the spatial distribution of the NH_3 emission roughly anticorrelates with both the bay and the ^{12}CO outflow. This NH_3

[6] Myers, Linke, and Benson (1983) identified two extinction maxima, L43B and L43E, in the obscuration immediately to the east of RNO 91. Only one NH_3 core was subsequently found in the area (Myers and Benson 1983); its position is near to but not coincident with either extinction maximum. Therefore we recommend that hereafter the core be identified only by the parent cloud L43 and that the suffixes B and E be dropped.

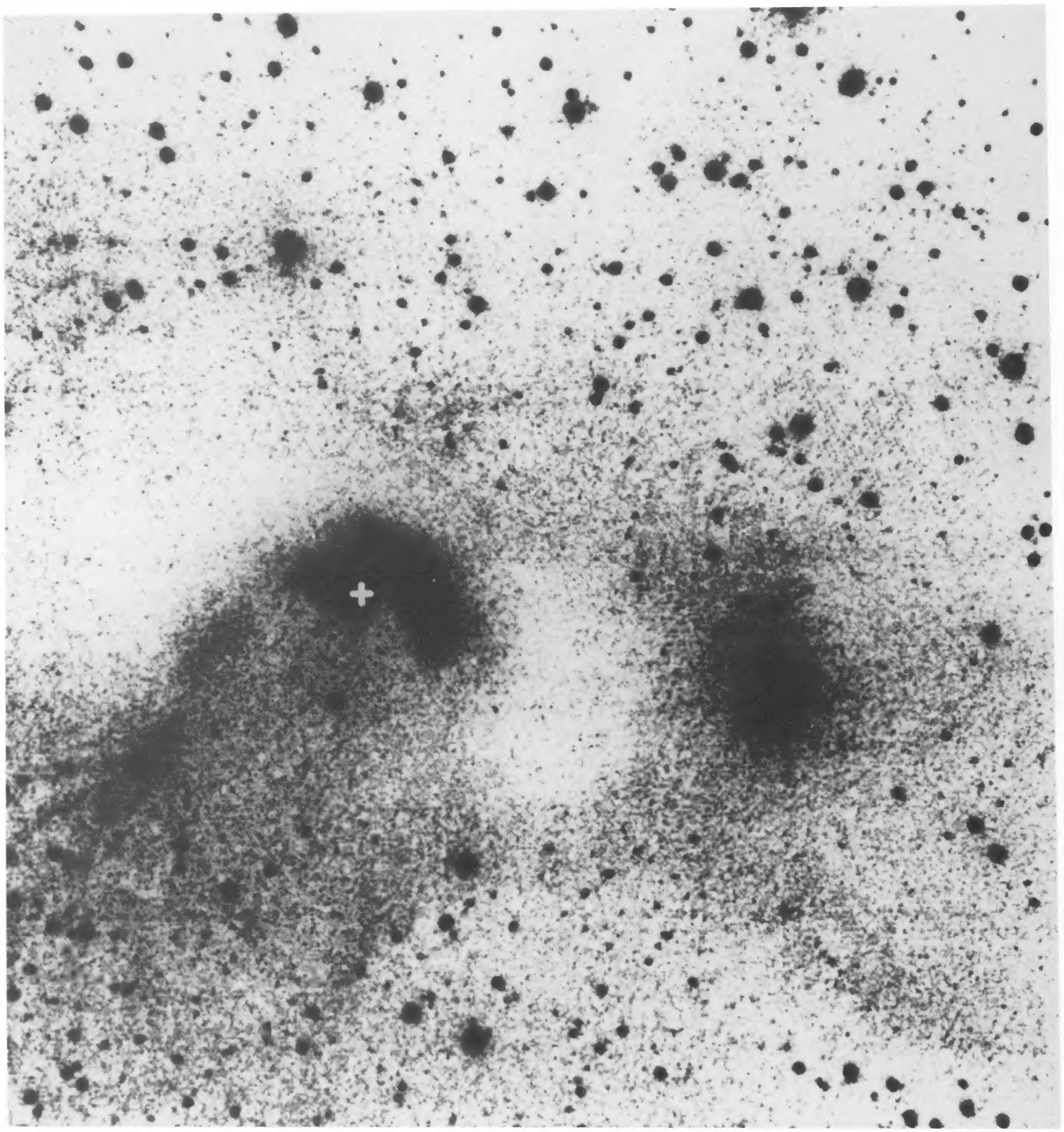

FIG. 1.—CCD *I* band image (12.4 arcmin square) of the RNO 90/91 region obtained with the FLWO 0.6 m at a scale of 1.46 arcsec pixel^{-1}. East is to the left and north to the top. RNO 91 is marked by the cross.

MATHIEU *et al.* (*see* **330**, 387)

PLATE 14

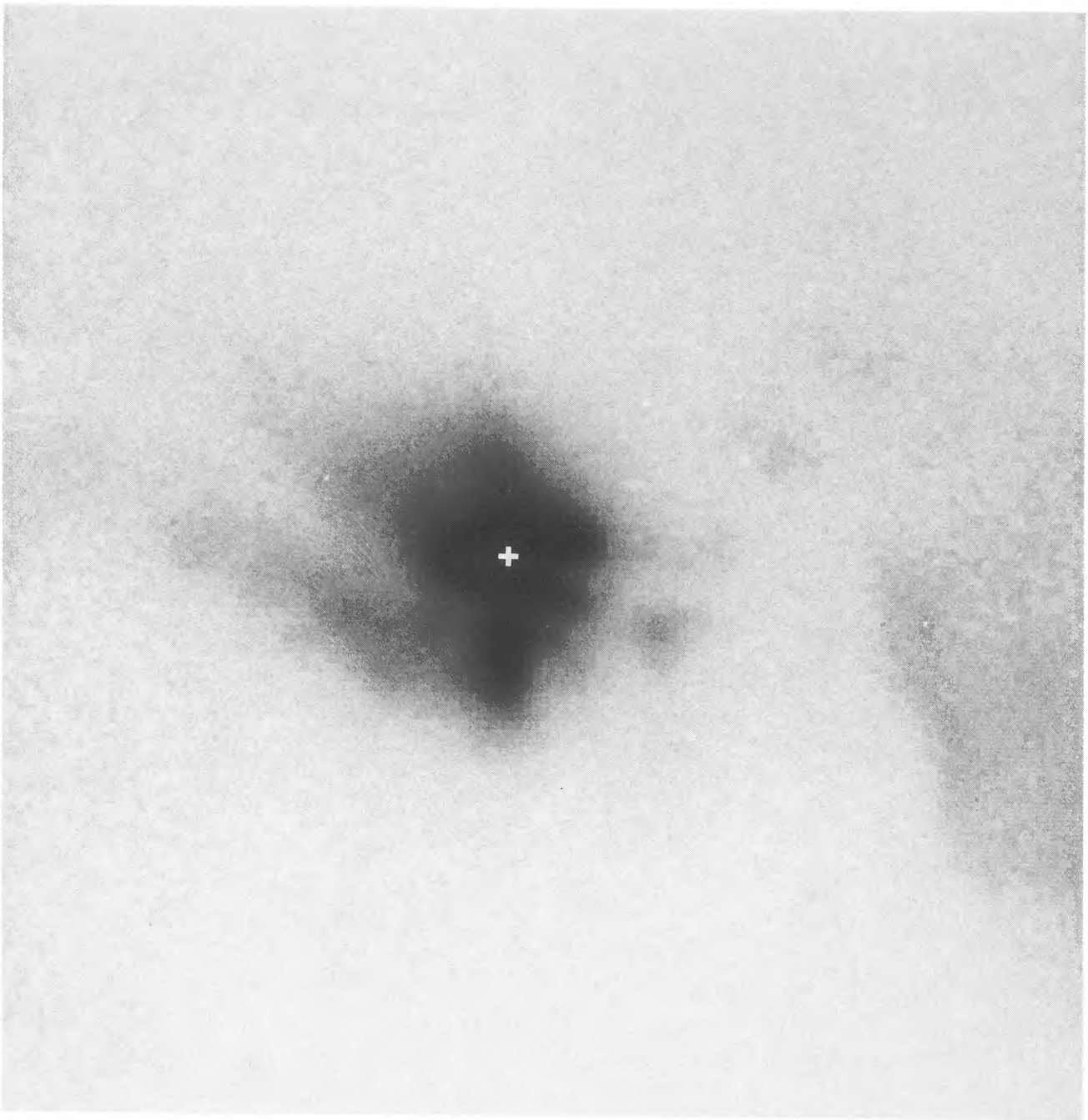

FIG. 2.—CCD *I* band image of RNO 91 obtained with the FLWO 0.6 m at a scale of 0.73 arcsec pixel^{-1}. East is to the left and north to the top. RNO 91 is marked by the cross.

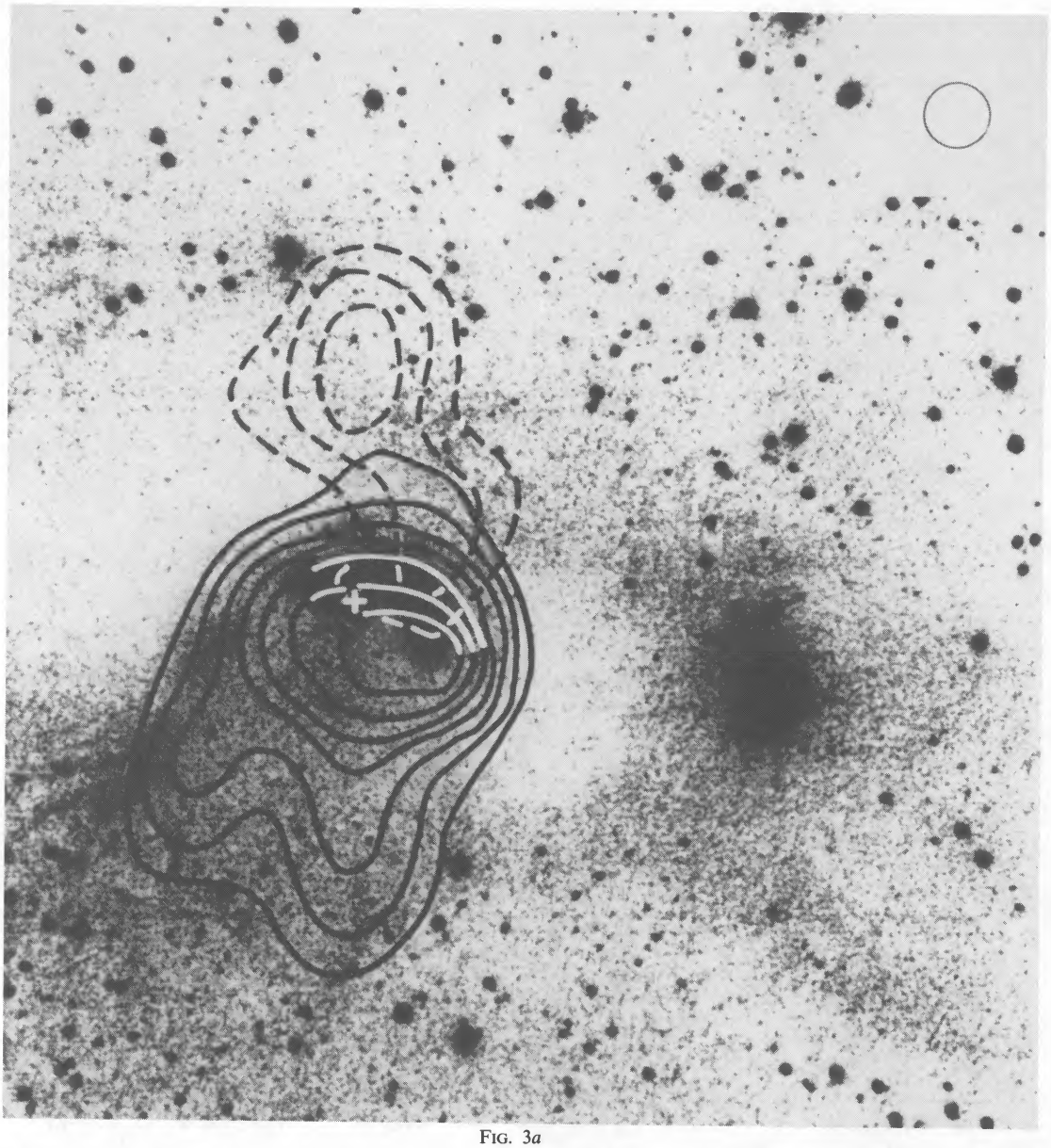

FIG. 3*a*

FIG. 3.—^{12}CO line wing, NH_3, and CS contour maps superposed on the CCD *I* band image presented in Fig. 1. The FWHM beam sizes are indicated in the upper right corner. RNO 91 is marked by the cross. (*a*) The ^{12}CO $J = 1$–0 line-wing intensity map has been taken from Myers *et al.* (1987). The contours indicate the ^{12}CO line intensity T_R integrated over the LSR velocity range -0.5 km s^{-1} to -4.5 km s^{-1} for the blue wing (*solid line*) and over the range 1.0 km s^{-1} to 5.0 km s^{-1} for the red wing (*dashed line*). The lowest contour is 3 K km s^{-1} with contours every 1 K km s^{-1}. (*b*) The NH_3 $(J, K) = (1, 1)$ contours indicate the peak line intensity T_A* of the main hyperfine component in intervals of 0.2 K, the lowest level being 0.2 K. (*c*) The CS (2–1) contours indicate peak line intesity T_R* in intervals of 0.3 K, the lowest level being 0.3 K.

distribution around RNO 91 is notably different from that found around IRS 5 and the L1551 outflow (Menten and Walmsley 1985), where the large-scale NH_3 emission is coincident with and elongated along the axis of the outflow.

In contrast, the peak antenna temperature of the CS emission is coincident with RNO 91 in projection (Fig. 3*c*); the integrated CS emission also peaks at RNO 91. This result is similar to that found by Heyer *et al.* (1986) at seven other sites of star formation. The distribution of the CS emission reflects the distribution of high extinction about RNO 91, with the highest intensity emission defining a ridge running from the patch of extinction to the west through RNO 91 to the large cloud to the east. CS emission is present throughout the bay; there is some curvature in the contours which reflect the shape of the bay. The CS emission is notably more extended than the NH_3 emission, being detectable beyond the outer boundaries of the extinction. Taking the geometric mean of the major and minor axis of two-dimensional Gaussian fits to the CS and NH_3 maps, the extent of the CS emission is 5.'4 (0.25 pc) as compared to the 3.'6 (0.17 pc) extent of the NH_3 emission.

The notable difference both in extent and peak of the NH_3 and CS emission distributions is not straightforward to explain since the critical density for CS (2–1) is 5.7×10^5 cm^{-3} as compared to 1.2×10^4 for NH_3. The spatial distribution of the

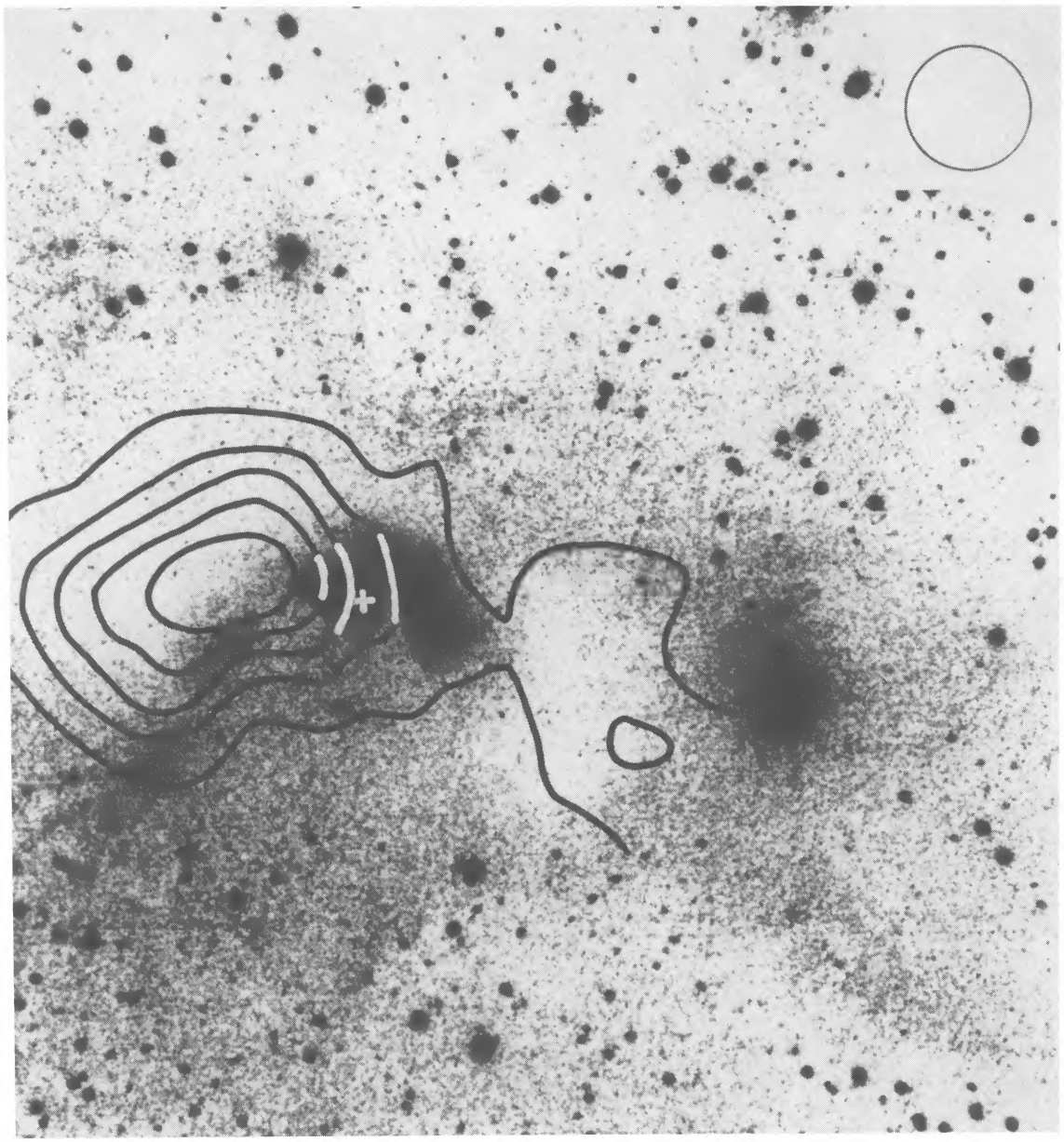

FIG. 3*b*

CS emission about the L43 core is similar to that of $C^{18}O$ (G. A. Fuller, in preparation) and ^{12}CO emission (Elmegreen and Elmegreen 1979), both tracers of low-density gas. Fuller and Myers (1987) suggest that CS emission from the dense core is scattered by CS molecules in the lower density material around the core; the NH_3 emission from the core may be scattered less because the line optical depth outside the core in NH_3 is less than in CS. If this picture is correct, then the CS emission in Figure 3*c* would be tracing lower density gas than the NH_3 emission.

This wealth of data permits a rather detailed description of the spatial relationship of the star, the outflow, and the dense molecular core. RNO 91 is located at the intersection of the blueshifted and redshifted lobes of the outflow, suggesting that the star is the likely source of the outflow. Given the extremely close projected spatial coincidence of the blue lobe of the CO outflow emission and the optical bay, the conclusion that the two are cospatial seems certainly correct. The parabolic contour of the projected outline of the bay suggests a roughly paraboloidal shape to the blueshifted outflow volume, similar to the schematic picture developed earlier for the L1551 outflow (e.g., Snell, Loren, and Plambeck 1980). The inclination to the line of sight and the opening angle of the outflow volume are difficult to determine precisely. In projection, the blue and red lobes are well separated and RNO 91 is located near the rear of the optical bay, suggesting that the inclination angle is small. Nonetheless, RNO 91 is projected within the boundaries of the bay, requiring the outlow to have either a large inclination angle, opening angle, or a combination of the two. [L1551 IRS 5, for example, is in projection located at the

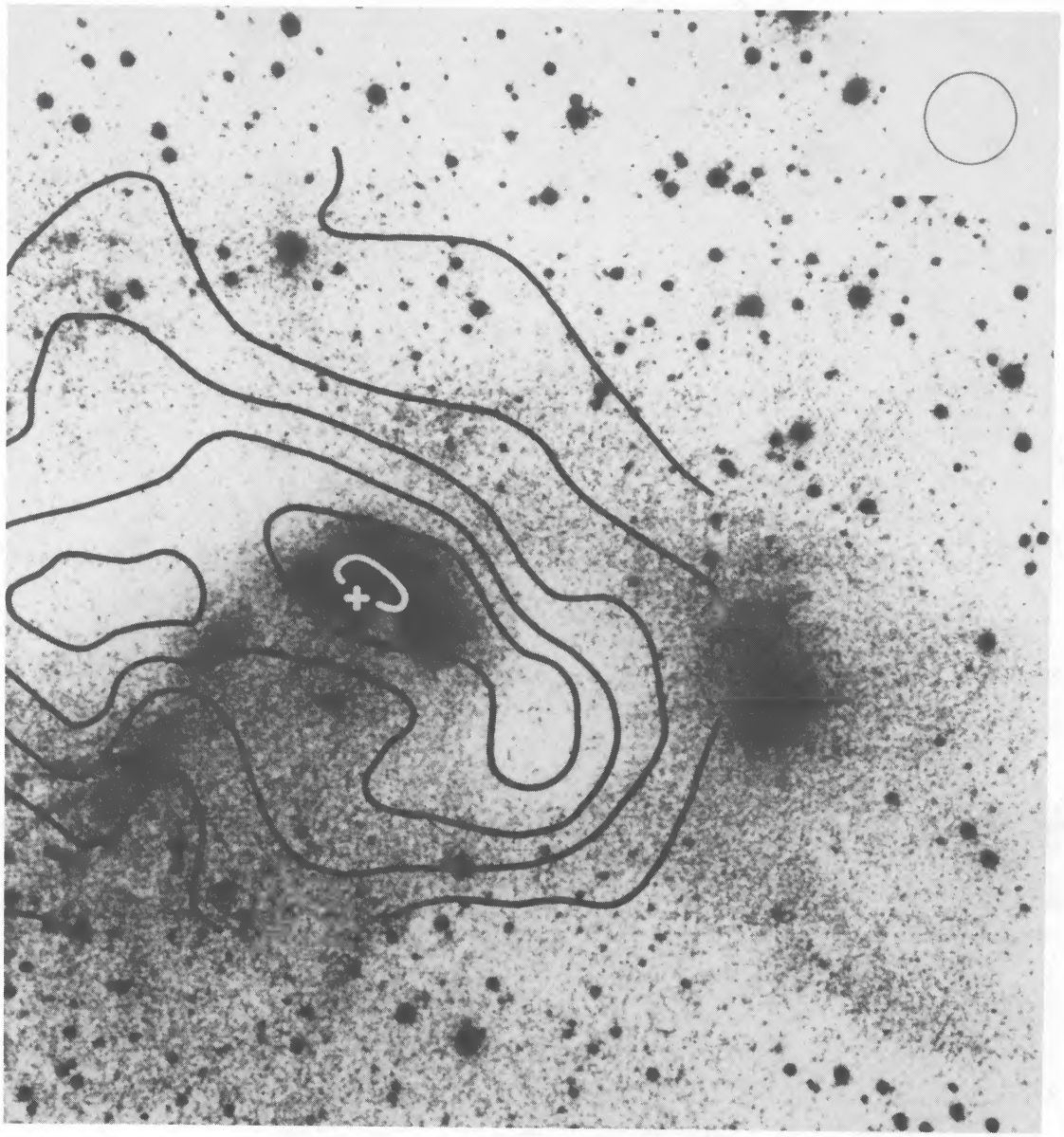

FIG. 3*c*

apex of the optical outflow volume and has an inclination angle estimated at roughly 15° (Snell *et al.* 1985).] The opposing constraints on the inclination angle suggest an intermediate inclination angle (20°–50°) and a large opening angle for the outflow near or at the star. One possible geometry is shown in Figure 4.

Extensive NH_3 emission surrounds RNO 91 and the outflow. In conjuction with the presence of reflection nebulosity both along the eastern wall and to the rear of the bay, these data indicate that RNO 91 and the outflow are embedded within a core of dense gas. Based on a somewhat less extensive NH_3 map, Myers and Benson (1983) derive a mass for this core of 0.7 $M_\odot$ within the FWHM radius of the NH_3 emission. (The Myers and Benson value for the mass has been corrected here for an error of a factor 3 in that paper. The FWHM radius and volume density derived from the new NH_3 observations presented here are not substantially different from those used by Myers and Benson.) We interpret the 0.07 pc offset between RNO 91 and the peak of the NH_3 emission as evidence for an offset between the star and the density maximum of the core of dense gas (see, for example, Fuller and Myers 1987); however, Menten *et al.* (1984) and Menten and Walmsley (1985) have interpreted smaller offsets in B335 and L1551 as a relative depletion of NH_3 in the dense circumstellar gas.

While extensive NH_3 emission surrounds RNO 91, NH_3 emission is notably absent in the southern half of the bay between the eastern and western regions of high extinction. In addition, Levreault (1988) estimates an extinction of only $A_v =$ 0.3 mag toward RNO 91 (but see also Myers *et al.* 1987). Finally, the surface brightness in the interior of the optical bay is uniform, with no indication of patchy extinction. These facts indicate that the outflow has displaced most of the extincting material along the line of sight to RNO 91 and that the outflow

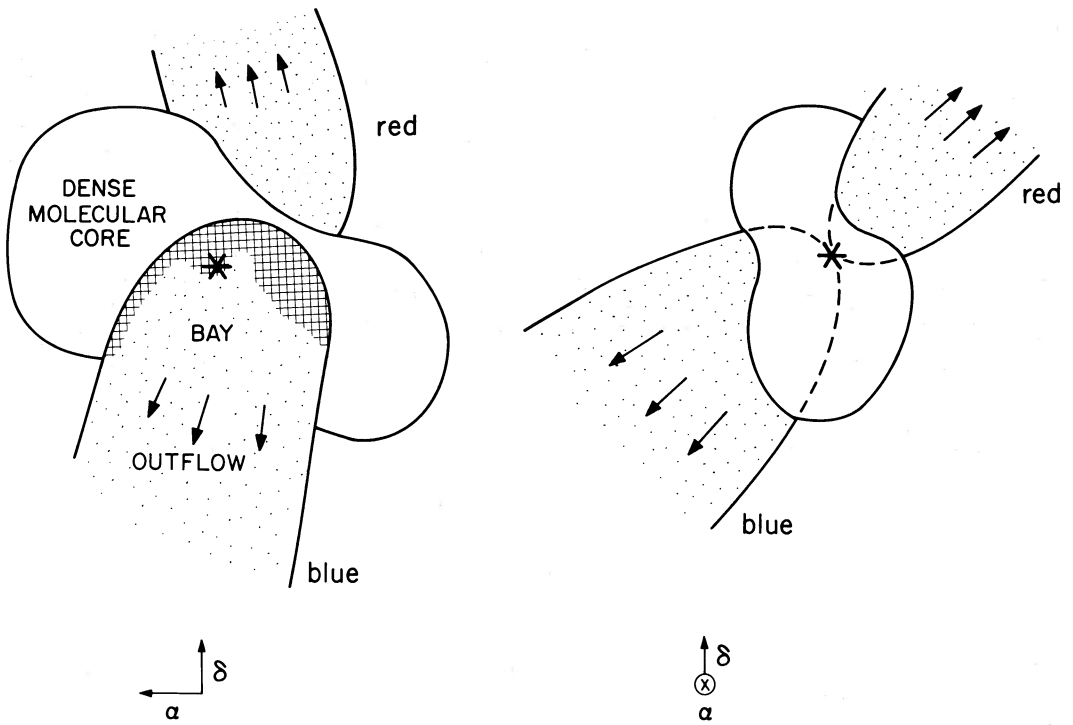

FIG. 4.—A schematic representation of the morphology of the RNO 91 region, as actually observed and as seen from a perspective 90° to the west of our line of sight. The speckled regions map molecular outflow, the hatched regions map reflection nebulosity, and the interior blank regions map dense molecular gas. The position of RNO 91 is marked by the star.

has emerged from the core within which RNO 91 was embedded. Note that Myers *et al.* (1988) estimate a total mass for the molecular outflow of 0.1 $M_{\odot}$, reasonably consistent with the total core mass and the relative sizes of the bay and the present core. The extension of the obscuration and surface brightness beyond the mouth of the bay may be due to material moved out of the bay by the action of the outflow, although it also may be more extended dust preferentially illuminated due to lower optical depth in the outflow volume. While the morphology of the volume associated with the redshifted lobe of the outflow is unknown, the furthest limit of this lobe is observed to be projected upon a relatively unobscured star field north of the filament, so that we can say that the redshifted flow is also not confined within the dense core.

To summarize, we present in Figure 4 a schematic picture of the morphology of the L43 core. In broad strokes the morphology reflects most of the features now typically attributed to bipolar outflow regions, specifically a young star at the common apex of two roughly paraboloidal volumes (within which lies the material associated with the CO outflow), all embedded within a dense molecular core. Although not shown in the figure, we envision the entire complex to be surrounded by a more extended cloud of lower density material, as traced by the ^{12}CO emission (and perhaps the CS emission). In detail, the L43 region is notable among dense molecular cores in that (1) the structure of the surrounding dense core has been visibly modified by the outflow and (2) the outflow has erupted beyond the boundaries of the core.

Finally, we compare the L43 and L1551 outflow regions, the latter having been the subject of extensive study (e.g., Snell, Loren, and Plambeck 1980; Kaifu *et al.* 1984; Snell *et al.* 1985; Menten and Walmsley 1985; Snell and Schloerb 1985). The L43 outflow is one of the weakest outflows yet detected. Thus in comparison the L1551 outflow is 5 times larger and ~10 times more massive, has ~40 times as much momentum, and is ~60 times more energetic than the L43 outflow (Snell and Schloerb 1985; Myers *et al.* 1988). The greater power of the L1551 outflow can likely be attributed to the higher luminosity of the source IRS 5; the *IRAS* luminosity of IRS 5 is 10 times greater than that of RNO 91 (Beichman *et al.* 1986) and the stellar mass-loss rate is 80 times greater (Snell and Schloerb 1985; Myers *et al.* 1988). Despite these differences in scale, however, the morphological similarities of the two regions are notable. The outflows in both regions are bipolar and well collimated, with young stellar objects located at the intersection of the red-shifted and blueshifted lobes. Both have associated optical structures, roughly parabolic in shape and very closely coincident with the blue lobes of the respective CO outflows. IRS 5 is located at the apex of the parabolic nebulosity in L1551, while RNO 91 lies near the rear of but still within the optical bay. The surface luminosity within the L43 bay is uniform, while most of the optical luminosity in L1551 is associated with the outflow volume more distant from IRS 5. However, these last two differences in detail can be easily understood as the consequence of different viewing angles. The schematic picture of L43 presented in Figure 4 with a viewing angle of 90° to the line of sight to L43, would serve well for L1551 as actually viewed. Finally, both regions have associated molecular cores of comparable mass from which the outflows have erupted. In conclusion, then, the two regions are notably similar in morphology except for the differences in scale. Since the dynamical lifetime of the L43 outflow is twice that of the L1551 outflow (Myers *et al.* 1988; Snell and Schloerb 1985), yet the L43 core does not show evidence of interaction with an outflow of comparable magnitude, to the L1551 outflow, it is unlikely that the differences in scale between the regions is due

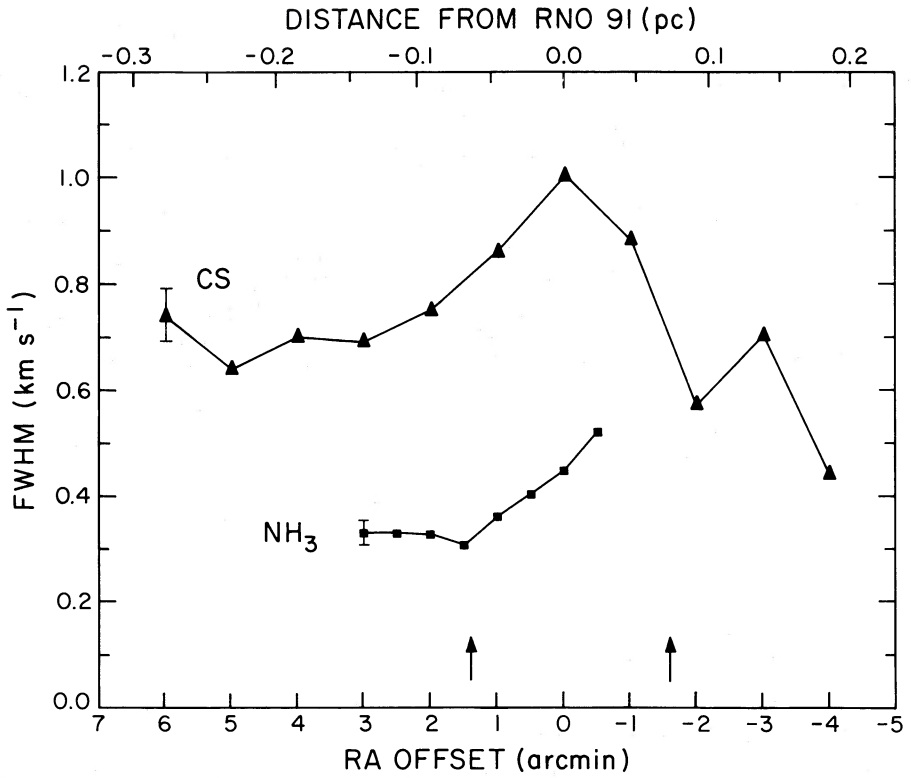

FIG. 5.—The run of FWHM line widths for CS and NH_3 along a declination track passing through RNO 91. Offsets are measured from the position of RNO 91 here and in the following figures. The error in a single NH_3 line width measurement is ~ 0.02 km s^{-1}. The typical error in a single CS line width measurement is ~ 0.05 km s^{-1}. Both are indicated by representative error bars. The edges of the bay are delineated by arrows.

to evolution. Thus the interaction between molecular outflows and dense cores, as depicted by the present states of both the L43 and L1551 regions, may be a typical evolutionary stage in the formation of low-mass stars, more or less independent of stellar luminosity or mass.

IV. KINEMATICS

a) Description

The morphological picture of the L43 core presented in § III shows that there has been sufficient interaction between the outflow and the material surrounding RNO 91 to substantially modify the spatial distribution of the surrounding material. It is reasonable to suspect that this energy and momentum transfer has produced increased turbulence, systematic motions, or both within the interacting material. The molecular line data presented here were obtained at sufficiently high velocity and spatial resolution to permit an examination of the kinematics in the region.

We consider first the variation of the NH_3 and CS line widths with position. Line widths of single NH_3 hyperfine components were determined from multi-component Gaussian fits with the procedures of Myers and Benson (1983); we use here only the high signal-to-noise data obtained at Effelsberg. We present in Figure 5 the run of FWHM with right ascension. Except for the two points farthest to the east which were observed along only the center track, each point is the average of line widths obtained along three tracks in declination, one passing through the position of RNO 91 and the others 0.5 (0.23 pc) north and south of this line. The intervals in right ascension are also 0.5. The error in a single line width measurement is ~ 0.02 km s^{-1}. The rms deviations derived from the three measurements at each right ascension position are somewhat larger, with a maximum of 0.08 km s^{-1} at the star. We also present in Figure 5 the run of the FWHM line widths of the CS (2–1) line with right ascension, along a single track passing through the position of RNO 91. Here the line widths were measured from single-component Gaussian fits to the lines; the typical 1 σ measurement error is 0.05 km s^{-1}. The CS line widths are approximately twice as large as the NH_3 line widths; the range from 0.6 to 1 km s^{-1} is comparable to the smallest mean line widths found by Heyer *et al.* (1986) in seven other star-forming regions.

Both the NH_3 and the CS line widths show a marked increase in the vicinity of RNO 91. The maximum CS line width along this track is observed at the position of RNO 91. The maximum NH_3 line width is observed 0.5 west of RNO 91, but the behavior of the NH_3 line widths farther to the west is not known because of the low signal-to-noise ratio of the Haystack spectra obtained there. We have also noted in Figure 5 the points where the track of observations crosses the boundaries of the optical bay and the CO outflow. The onset of increasing NH_3 line width coincides with the eastern boundary of the outflowing material. The CS line widths also begin to increase approximately at the boundaries of the bay and outflow. Thus there is a close association between the bay and the increased line widths.

The extensive CS map permits a two-dimensional perspective on the spatial distribution of line width. In Figure 6 we present the contour map of CS line width superposed upon the 4 K contour of the ^{12}CO wing maps presented in Figure 3*a*. The minimum CS line width contour shown is 0.9 km s^{-1}, so we have emphasized sites of large line width. The spatial coin-

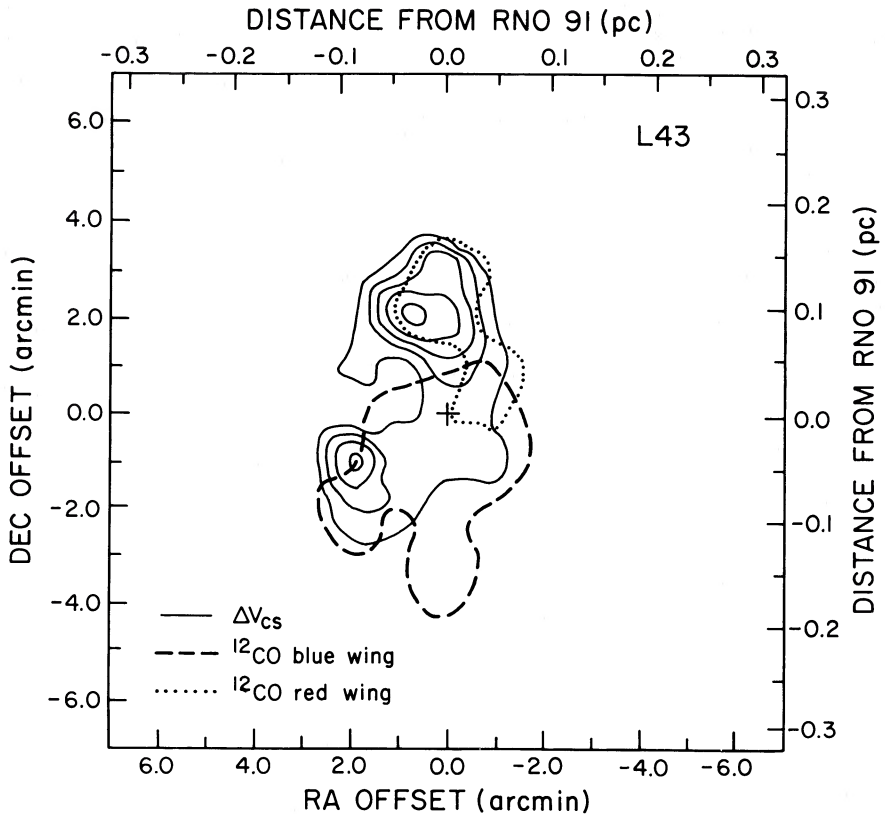

FIG. 6.—Contour map of CS velocity width in intervals of 0.2 km s^{-1}, the lowest level being 0.9 km s^{-1}. Also shown are the 0.4 K contours of the ^{12}CO blue-wing and red-wing emission. RNO 91 is marked by the cross.

cidence of the broad CS lines and both lobes of the ^{12}CO outflow over the entire domain of the outflow is striking. The maximum CS line widths (~ 1.6 km s^{-1}) are associated with regions of the outflow well removed from RNO 91 itself. The peak in the line width distribution associated with the blue lobe of the outflow is seen at only one observed position, but the maximum to the north extends over several positions.

There is also substantial structure in both the NH_3 and CS velocity fields. In Figure 7 we have plotted the NH_3 line centers as a function of position, again along a track in right ascension through RNO 91. The positions marked by filled squares are derived from the Effelsberg data averaged in the same way as the line width data. The open squares indicate line centers for positions observed only at Haystack along a single right ascension track through RNO 91. The Haystack line centers are derived from Gaussian fits to the main hyperfine components. The agreement between the Effelsberg and Haystack data at common positions was good; only the Effelsberg data are shown. We also present in Figure 7 the CS line center velocities along a right ascension track passing through RNO 91; the line centers were determined by Guassian fits, although the line centroids produced similar results. The NH_3 and CS velocity fields agree well.

The significant feature seen in the NH_3 and CS velocity fields is a steep gradient immediately to the east of RNO 91. Beyond 1.5 (0.07 pc) east of RNO 91 the velocity field is roughly constant at 0.7–0.8 km s^{-1}. However, at 1.5 a steep gradient begins, with a slope of ~ 3.5 km s^{-1} pc^{-1} between this point and the star. To the west of RNO 91 the NH_3 velocity field again remains roughly constant at 0.4–0.5 km s^{-1}. This gradient in the velocity field is very similar to that seen by Menten and Walmsley (1985) in the vicinity of IRS 5 and to several gradients seen in other dense cores (Myers, Goodman, and Benson 1988).

In Figure 8 we present a contour map of the two-dimensional CS velocity field. The velocity gradient seen in Figure 7 is in fact an extended slope in the velocity field. We have fitted a plane to the CS velocity-position data within a 5 arcmin square box centered 1′ north and east of RNO 91. The fit is quite good, with the gradient lying at a position angle of $26° \pm 5°$ and having a slope of 2 km s^{-1} pc^{-1}. The direction of the gradient is shown in Figure 8. A similar fit done to the Haystack NH_3 velocity field in the same region finds a gradient at a position angle of $-1° \pm 12°$ and a slope of 2 km s^{-1} pc^{-1}.

Unlike the spatial distribution of the CS line widths, the two-dimensional CS velocity field does not show a close relationship with either the optical morphology or the outflow velocity field. While the projected position of the velocity gradient passes through the bay and outflow, the velocity field does not change notably at the bay and outflow boundaries. The direction of the gradient is similar to that of the axis of the bay and the blue lobe of the outflow. However, the sense of the gradient is reversed from that of the outflow velocity field; the most blueshifted CS and NH_3 emission is projected upon the redshifted wing of the outflow. The direction of the gradient is also perpendicular to the large-scale axis of the L43 filament, perhaps surprising if the elongation of the filament is attributed to magnetic fields aligned perpendicular to the elongation. However, Heyer *et al.* (1986) also have found numerous CS velocity gradients and note a general lack of correlation

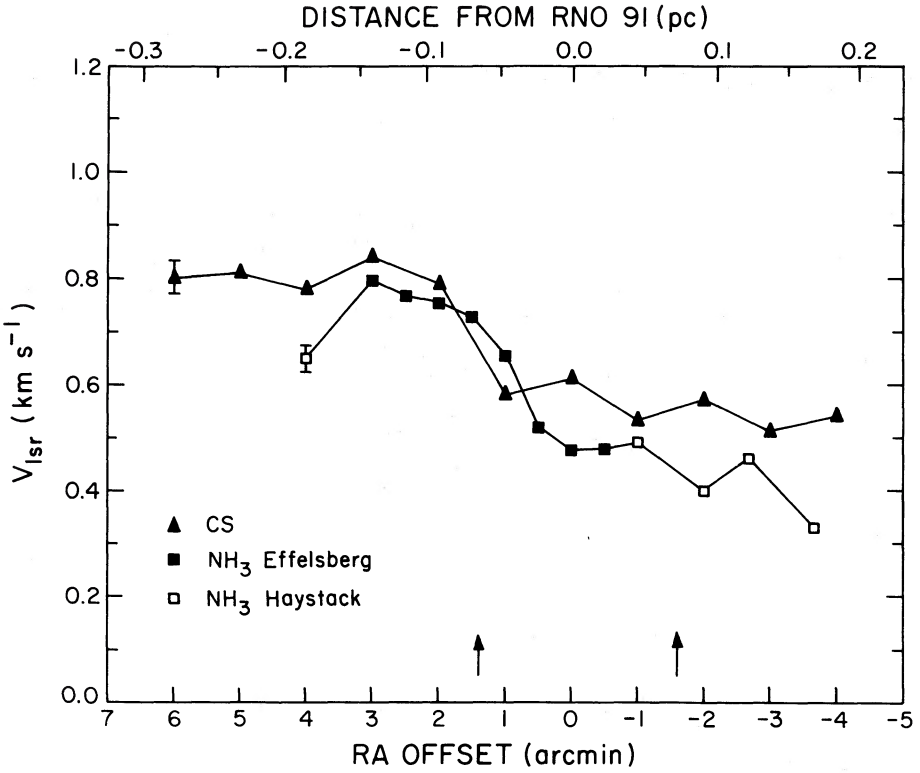

FIG. 7.—The run of V_{lsr} for CS and NH_3 along a declination track passing through RNO 91. The open boxes show NH_3 measurements obtained at Haystack; the filled boxes show NH_3 measurements obtained at Effelsberg. The typical error in a single NH_3 line center measurement is ~ 0.02 km s^{-1}; the typical error in a single CS line center measurement is ~ 0.03 km s^{-1}. Both are indicated by the representative error bars. The edges of the bay are delineated by arrows.

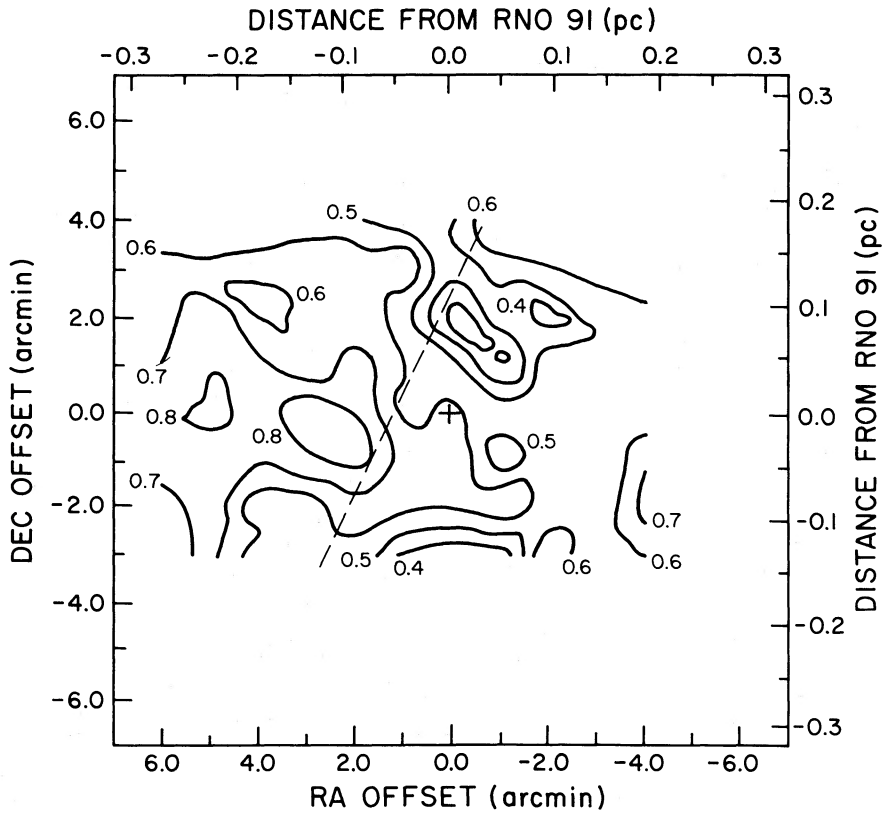

FIG. 8.—Contour map of CS line center velocity in intervals of 0.1 km s^{-1}, the lowest level being 0.2 km s^{-1}. The best-fit linear velocity gradient is marked by the dashed line. RNO 91 is marked by the cross.

between these gradients and the corresponding cloud morphologies.

b) Discussion

Both the NH_3 and CS line-width data indicate the presence of relatively local disturbances in the motions of the core material in the vicinity of RNO 91 and the associated outflow. The close spatial coincidence of the CO outflow and the increased molecular line widths, particularly for the CS emission as shown in Figure 6, clearly point to the outflow as the source of the disturbance. The issue then becomes the nature of the interaction between the outflow and the ambient gas.

The most straightforward explanation for the increased line widths is that the systematic outflow motions seen in ^{12}CO are also traced by NH_3 and CS emission. This might be expected, for example, if the NH_3 and CS emission arose from clumps entrained in the outflow. This explanation would attribute the increased line widths to the presence of wings on the emission-line profiles. In fact, however, the data do not support this picture. There is no evidence for wings or asymmetries in the NH_3 line profiles. However, Menten *et al.* (1984) show that, for normal molecular cloud abundances, NH_3 emission with velocities corresponding to molecular outflow wings would not be detectable. Thus the fact that line broadening is observed actually suggests that the broadening is not due to emission from dense material entrained in the outflow. Indeed, the increase in the NH_3 line widths of only a few tenths of a km s^{-1} is significantly smaller than the outflow velocities of several km s^{-1}. However, if the dense gas is clumped, it is possible that the systemic clump velocities may be less than the outflow velocity of the lower density gas.

Snell and Schloerb (1985) detect both redshifted and blueshifted high-velocity components in their CS observations of the L1551 outflow. We have examined the L43 and CS spectra at 30 kHz resolution (obtained simultaneously with the 100 kHz observations). In order to obtain sufficient signal-to-noise, we have combined six adjacent spectra about each of two positions, one north and one south of RNO 91 within the outflow boundaries. The averaged spectra are shown in Figure 9. At the position south of RNO 91 there is no evidence for any asymmetry in the line profile; however fitting two Guassians to the line profile indicates both a narrow (FWHM = 0.9 km s^{-1}) and a weaker broad (FWHM = 1.5 km s^{-1}) component with the same line-center velocity. North of RNO 91 the composite spectrum does have an asymmetric line profile suggestive of multiple velocity components. However, the shape of the CS line profile is very different from the ^{12}CO line profile north of RNO 91 (Myers *et al.* 1988), most notably in that the sense of the asymmetry is reversed. In addition, there is a dip in the CS line profile near the NH_3 line-center velocity of 0.5 km s^{-1} (averaged over the same positions). Thus the line structure may be indicative of self-absorption of CS rather than separate velocity components associated with the outflow. In summary, then, the CS line profiles do not show asymmetries similar in shape or magnitude with the ^{12}CO line profiles. Nonetheless, there is evidence for structure in the line profiles and higher signal-to-noise data, as well as observations in other transitions of CS, are warranted.

The most serious difficulty with the interpretation of the increased line widths as due to entrained material is the lack of correlation between the CS velocity field and the outflow velocity field. When line asymmetries are not resolved, systematic motions due to the outflow should also produce systematic

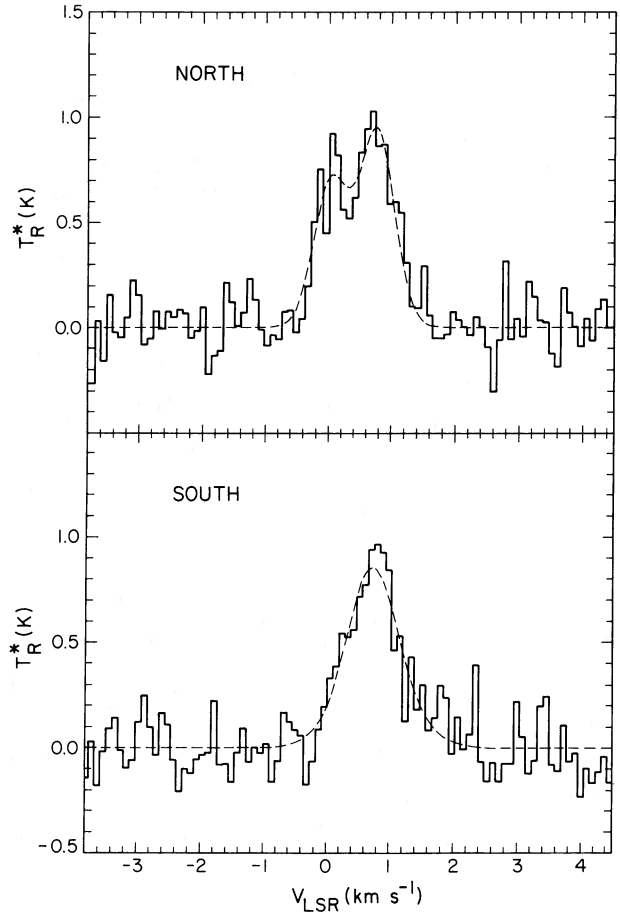

FIG. 9.—Averages of six CS spectra (30 kHz resolution) about central positions projected within the red and blue lobes of the ^{12}CO outflow. Dashed lines show best fits of two Guassians. (*a*) Average of spectra at positions of ($\Delta\alpha = -1$, $\Delta\delta = 1$), (-1, 2), (0, 1), (0, 2), (1. 1). and (1, 2). Offsets are in arcmin with respect to position of RNO 91. (*b*) Average of spectra at positions (0, -1), (0, -2), (1, -1), (1, -2), (2, -1), and (2, -2).

shifts in the NH_3 and CS line-center velocities in the same sense as the motions of the outflow. In fact, however, we have noted that the gradient seen in the NH_3 and CS velocity fields actually has the opposite sense from the CO outflow; the most blueshifted emission is projected upon the redshifted lobe of the outflow. Thus there is no evidence in the structure of either the NH_3 or CS velocity fields suggesting that the line widths might be due to systematic velocities resulting from the outflow motions.

The data are more consistent with the interpretation that the increase in line widths within the outflow boundaries arises purely from increased turbulence (i.e., unordered motions) resulting from interaction between the outflow and the surrounding cloud. This interaction may take the form of instabilities where highly supersonic material flows past the ambient gas, or more dramatically, collision between the outflow and dense clumps or surrounding dense material. The observational signature of increased turbulence would be symmetrically broadened line profiles, perhaps with a narrower component as well arising from the undisturbed material along the line of sight. The southern profile presented in Figure 9 agrees well with this prediction; the interpretation of the northern profile is less clear.

Assuming the NH_3 line widths derive entirely from thermal and turbulent motions in a single component, we can estimate the increase in turbulent velocity due to the outflow. The line widths of 0.3 km s^{-1} at points far from both RNO 91 and the CO outflow are typical of the line widths found in cores which do not contain either an embedded *IRAS* source or an outflow. According to the procedure of Myers *et al.* (1988), and assuming a kinetic temperature of 10 K,[7] these quiescent line widths indicate a nonthermal velocity component of 0.22 km s^{-1}. The maximum observed NH_3 line width is 0.52 km s^{-1}. Given the small variation in temperature across the Effelsberg map, this increase in line width can be attributed entirely to nonthermal motions, in particular a nonthermal velocity component of 0.47 km s^{-1} at the NH_3 line-width peak. Note that this is only a rough estimate since the NH_3 lines are likely to be composites of two components, one broad-lined arising from gas disturbed by the outflow and the other narrow-lined arising from quiescent gas in the core located along the line of sight behind the outflow. Even with this uncertainty, the data indicate that the typical nonthermal motions within the disturbed dense gas are a factor 2 greater than in the undisturbed gas.

CS emission lines observed far from the outflow show velocity widths of 0.6 km s^{-1}. Such widths are far larger than expected from thermal motions. Within the projected boundaries of the outflow most of the CS line widths are ~ 1 km s^{-1}, with the maximum CS line widths observed being as high as 1.6 km s^{-1}. This increase in line widths is substantially greater than found in the NH_3 emission, additional evidence that the emission from the two molecules is not tracing the same density material. The observation that the outflow has been more effective in disturbing the material giving rise to the CS emission is consistent with the hypothesis that the CS emission is tracing gas at lower densities than the NH_3 emission, since the effectiveness of the coupling between outflow and ambient material would be expected to increase as the density contrast decreases.

Interestingly, the two positions of maximum line width, one projected against the blue wing and one against the red wing, are of order 0.1 pc distant from RNO 91. The substantial increase in line width and the spatial confinement of these line width maxima relative to the size scale of the outflow are suggestive of the possibility that at these positions the outflow is plowing directly into the surrounding gas. If the outflow has already erupted from the densest regions of the core, as suggested by the optical morphology, then one might expect to see the maximum disturbance only in the tracers of lower density gas.

In summary, then, the present evidence suggests that the NH_3 and CS line broadening is dominated by increased turbulent motions driven by the outflow. It is curious that the interaction of the outflow with the core material is sufficient to substantially increase the turbulence of the material, and yet the emission provides no evidence for entrainment of the interacting dense material. The lack of evidence for systematic motion may be indicative of changes in the physical conditions of swept-up dense material, inhibiting NH_3 and CS emission. Finally, we note that Menten and Walmsley (1985) find a similar increase in NH_3 line widths around IRS 5. However, they find increased line widths associated only with the redshifted outflow; the line widths projected upon the blueshifted flow are typical for quiescent clouds. They suggest that this indicates that interaction is occurring only with the background cloud; as with L43, however, there is evidence in the L1551 optical morphology of interaction associated with the blueshifted flow.

The relation, if any, between the gradient in the NH_3 and CS velocity fields and the outflow and the formation of RNO 91 is less clear. The narrow-lined NH_3 and CS emission projected upon the extinction to the east and west of the outflow show a velocity difference of 0.3–0.4 km s^{-1}, corresponding to the respective limiting velocities of the velocity gradient. Since there is no evidence that these regions of the core have been disturbed, the evidence indicates that a gradient existed prior to the formation of RNO 91 or the outflow. Such gradients are often interpreted as evidence for rotation. In this interpretation, the projected axis of rotation, derived from the CS velocity field, would lie at a position angle of 116°, as compared to the position angle of the outflow axis of 25°. This orientation suggests that this large-scale rotation is not associated with the collimation of the outflow, a conclusion also drawn by Heyer *et al.* (1986) on similar grounds for several other regions. On the other hand, RNO 91 lies in projection within the velocity gradient and the inferred rotation axis would pass very near RNO 91. Also, with respect to the L43 cloud as a whole, the velocity gradient is a very small-scale feature in the vicinity of RNO 91; the distance between velocity extremes is only 0.2 pc. Both of these facts suggest an association between the velocity gradient and the formation of the star.

V. CONCLUSION

CCD images reveal a bay in the dark cloud L43, within which lies the very young star RNO 91. The bay is in projection precisely coincident with the blue lobe of the ^{12}CO molecular outflow emission associated with RNO 91. NH_3 emission, tracing dense gas, follows the high extinction adjacent to the bay, but is absent within the bay except near RNO 91. The extinction through the bay to RNO 91 is small. Finally, the line widths of both the NH_3 and CS emission increase within the boundaries of the outflow and bay. This ensemble of observations blends together into one coherent picture in which the outflow originating at RNO 91 has blown through the dense core into the lower density environs, in the process revealing RNO 91 and the outflow cavity.

The detailed study presented here of this interaction between the L43 outflow and core has implications with regard to recent statistical studies of the interactions of cores, stars, and outflows and the general issue of how newly formed stars separate from their parent cores. Beichman *et al.* (1986) showed that dense molecular cores with embedded *IRAS* sources have both $C^{18}O$ and NH_3 line widths which are significantly larger than cores with either no *IRAS* source or an *IRAS* source associated with a visible counterpart. In particular, NH_3 line widths were shown to vary from 0.29 ± 0.02 km s^{-1} in cores without *IRAS* sources to 0.40 ± 0.4 km s^{-1} in cores with embedded *IRAS* sources. Since the thermal contribution to the line widths of these cores are all comparable, this increase in line width is due to additional nonthermal motions of cores with young embedded stars. Myers *et al.* (1988) have shown that cores with CO outflows, all of which in their survey had associated *IRAS* point sources, also typically have nonthermal line widths which are roughly 1.5–2 times larger than those

[7] Kinetic temperatures in L43 [derived from the Effelsberg data as in Myers and Benson (1983)] range from 9 to 15 K, the median being 11 K. The derived temperature at RNO 91 is 11.9 K.

cores without CO outflows. Myers *et al.* also show that the momentum and kinetic energies in these outflows are comparable to the momentum and kinetic energies of the cores. They conclude that a typical outflow causes a substantial increase in the internal momentum and kinetic energy of the associated core and further suggest that outflows are likely to be the main agents of core dispersal.

The detailed morphological and kinematic study of the L43 core clarifies several points of this picture. First, the data clearly show that the increased NH_3 line widths are indeed intimately associated with the CO outflow. Outside of the projected boundaries of the outflow the NH_3 line widths are ~ 0.3 km s^{-1}; within the boundaries they increase to ~ 0.5 km s^{-1} in the vicinity of RNO 91. Similarly, the close association of increased CS line widths with both the redshifted and blueshifted lobes of the CO outflow over distances up to 0.15 pc from the star in projection argues strongly that the molecular outflow is the source of the increased internal motions.

The data also show that, at least presently, the increased internal motions are present in only a limited volume of the L43 core. The outflow energy is coupled with only a limited fraction of the core mass; most of the mass in the L43 core is undisturbed. Thus these results emphasize that, while rough calculations of outflow and core momenta and energies suggest that outflows have energies comparable to their parent cores and thus may be the source of core dispersal (Myers *et al.* 1988), the issue of whether the outflow energy is actually deposited in the core remains critical to assessing whether the outflow in fact substantially disrupts the core. In addition, clearly, care must be taken when computing dynamical masses and total energies and momenta of molecular cores with outflows.

Second, the near perfect coincidence in projection of the blueshifted lobe of the outflow and the bay cut into the middle of the L43 core leaves little doubt regarding the capability of outflows to substantially alter the structure of a core. However, again, the outflow has by no mean modified or dispersed the entire parent molecular core. The dense molecular gas not yet disturbed by the outflow has size, mass, and internal motions comparable to those of quiescent molecular cores in which star formation has not recently taken place. Apparently the mechanical action of the outflow has been spatially restricted by its collimation, its enviroment, and possibly its youth.

If the assumption is made that stars form at the density maxima of their parent cores, the action of the outflow may explain the separation of 0.07 pc between RNO 91 and the peak of the NH_3 emission. However, other processes would, in conjunction or independently, also be expected to lead to an observed offset between a young star and the presently observed density maximum. The most straightforward process is simply the consumption of material to form a 0.5 $M_\odot$ star from an approximately solar-mass core; this redistribution of material will almost certainly alter the core structure. In addition, the star may have moved away from the density maximum since formation. For stars with ages of several times 10^5 yr or more, relative velocities comparable to the internal motions of the core would suffice to move a few hundredths of a parsec. In the case of L43, however, it seems unlikely that the star formed at the presently observed NH_3 peak. Myers *et al.* (1988) estimate a dynamical lifetime of the flow of 2×10^5 yr, comparable to the age of the star. However, the present NH_3 emission at the peak shows no morphological or kinematic evidence of having been disturbed. We conclude that, if RNO 91 indeed formed at a density maximum in the core, the core has been both sufficiently depleted of dense gas in the formation of the star and disrupted by the outflow so that the density peak has shifted.

Finally, we note that given the substantial disruption of the core immediately adjacent to RNO 91, it seems likely that the action of the outflow has reduced or possibly eliminated the supply of dense gas available for accretion onto the star. Indeed, the onset of the outflow may have been the mechanism dictating the final mass of RNO 91.

In conclusion, it is clear that the outflow has both increased the internal motions and modified the structure of the core surrounding RNO 91. Since L43 is one of the weakest outflows yet detected, it seems reasonable that similar outflow/core interactions are to be expected in any core with detected outflows. Furthermore, Myers *et al* (1987*b*) suggest that the frequency of detected outflows is high enough to imply that outflows are both common and long-lived features of star-core systems. We suggest, therefore, that at some stage in their evolution most cores in which young stars form pass through a stage analogous to the present state of L43, in particular a period when an outflow has reduced or terminated accretion and begun to disperse the core, exposing the newly formed star.

Whether the L43 outflow will be capable of completely disrupting the core is not clear. (A dense core as defined by NH_3 emission is part of a larger continuous structure; the size and existence of the dense core is somewhat a matter of convention. By disruption we mean essentially complete dispersal of the densest [$\rho > 10^4$ cm^{-3}] molecular gas). There is evidence that not all cores in which stars form are in fact largely or entirely disrupted on time scales less than millions of years. Beichman *et al.* (1986) note that cores associated with visible *IRAS* sources are very similar to those cores with no associated *IRAS* sources. They therefore suggest that the radius of influence of an unobscured star must be small (~ 0.2 pc) and the memory of a cloud core regarding the source of agitation must be short ($\sim 10^5$ yr). They also find that both cores without *IRAS* sources and cores with visible *IRAS* sources are roughly half the mass of cores with embedded *IRAS* sources. Our findings in L43 suggest that the cores with visible *IRAS* sources may simply be undisturbed remnants of the larger parent cores. Thus the outflow associated with RNO 91 may indeed not entirely disperse the L43 dense core, but rather only clear out the immediate environment of RNO 91, leaving the star associated with the remnant dense core.

We acknowledge valuable conversations with R. Levreault and R. Mundt. P. J. B. thanks K. M. Menten and C. M. Walmsley for assistance while observing at Effelsberg, In-Situ, Inc., for the contouring software, and the William and Flora Hewlett Foundation Grant of the Research Corporation and the National Science Foundation under grant AST86-10467 for support of this research. G. A. F. acknowledges support from NSF grant AST84-16177 to the Radio Astronomy Laboratory of the University of California, Berkeley, and from the Smithsonian Predoctoral Fellowship Program.

REFERENCES

Beichman, C. A., Myers, P. C., Emerson, J. P., Harris, S., Mathieu, R. D., Benson, P. J., and Jennings, R. E. 1986, *Ap. J.*, **307**, 337.
Benson, P. J., and Myers, P. C. 1980, *Ap. J.* (*Letters*), **242**, L87.
Campbell, B., Persson, S. E., and McGregor, P. J. 1986, *Ap. J.*, **305**, 336.
Cohen, M. 1980, *A.J.*, **85**, 29.
Elmegreen, D. M., and Elmegreen, B. G. 1979, *A.J.*, **84**, 615.
Fuller, G. A., and Myers, P. C. 1987, in *Physical Processes in Interstellar Clouds*, ed. G. Morfill and M. Scholer (Dordrecht: Reidel), in press.
Geary, J., and Kent, S. 1981, in *Solid State Imagers for Astronomy*, (*Proc. Soc. Photo Opt. Eng.*, **280**), p. 51.
Herbst, W., and Warner, J. W. 1981, *A.J.*, **86**, 885.
Heyer, M. C., Snell, R. L., Goldsmith, P. F., Strom, S. E., and Strom, K. M. 1986, *Ap. J.*, **308**, 134.
Kaifu, N., Suzuki, S., Hasegawa, T., Morimoto, M., Inatani, J., Nagane, K., Miyazawa, K., Chikada, Y., Kanzawa, T., and Akabane, K. 1984, *Astr. Ap.*, **134**, 7.
Kutner, M. L., and Ulich, B. L. 1981, *Ap. J.*, **250**, 341.
Levreault, R. M. 1984, *Ap. J.*, **277**, 634.
———. 1988, *Ap. J.*, submitted.
Loren, R. B. 1981, *A.J.*, **86**, 69.
Menten, K. M., and Walmsley, C. M. 1985, *Astr. Ap.*, **146**, 369.
Menten, K. M., Walmsley, C. M., Krügel, E., and Ungerechts, H. 1984, *Astr. Ap.*, **137**, 108.
Mundt, R. 1985, in *Protostars and Planets II*, ed. D. C. Black and M. S. Matthews (Tucson: University of Arizona Press), p. 414.
Myers, P. C. 1985, in *Protostars and Planets II*, ed. D. C. Black and M. S. Matthews (Tucson: University of Arizona Press), p. 81.
Myers, P. C., and Benson, P. J. 1983, *Ap. J.*, **266**, 309.
Myers, P. C., Fuller, G. A., Mathieu, R. D., Beichman, C. A., Benson, P. J., Schild, R. E., and Emerson, J. P. 1987, *Ap. J.*, **319**, 340.
Myers, P. C., Goodman, A., and Benson, P. J. 1988, in preparation.
Myers, P. C., Heyer, M., Snell, R., and Goldsmith, P. 1988, *Ap. J.*, **324**, 907.
Myers, P. C., Linke, R. A., and Benson, P. J. 1983, *Ap. J.*, **264**, 517.
Schild, R. E., and Kent, S. 1981, in *Solid State Imagers for Astronomy*, (*Proc. Soc. Photo Opt. Eng.*, **280**), p. 186.
Snell, R. L., Bally, J., Strom, S. E., and Strom, K. M. 1985, *Ap. J.*, **290**, 587.
Snell, R. L., Loren, R. B., and Plambeck, R. L. 1980, *Ap. J.* (*Letters*), **239**, L17.
Snell, R. L., and Schloerb, F. P. 1985, *Ap. J.*, **295**, 490.
Stahler, S. W. 1985, *Ap. J.*, **293**, 207.
Strom, K. M., Strom, S. E., Wolff, S. C., Morgan, J., and Wenz, M. 1986, *Ap. J. Suppl.*, **62**, 39.

P. J. BENSON: Department of Astronomy, Wellesley College, Wellesley, MA 02181

G. A. FULLER: Astronomy Department, University of California, Berkeley, CA 94720

R. D. MATHIEU: Department of Astronomy, University of Wisconsin, Madison, WI 53706

P. C. MYERS and R. E. SCHILD: Harvard-Smithsonian Center for Astrophysics, 60 Garden St., Cambridge, MA 02138